



Contents lists available at ScienceDirect

Journal of Inorganic Biochemistry

journal homepage: www.elsevier.com/locate/jinorgbio

Structure–activity relationship studies on rhodamine B-based fluorogenic probes and their activation by anticancer platinum(II) compounds

Jun Xiang Ong^a, Jian Yu Yap^{a,b}, Siew Qi Yap^a, Wee Han Ang^{a,b,*}

^a Department of Chemistry, National University of Singapore, 3 Science Drive 3, Singapore 117543, Singapore

^b NUS Graduate School for Integrative Sciences and Engineering, National University of Singapore, 28 Medical Drive, Singapore 117456, Singapore

ARTICLE INFO

Article history:

Received 15 May 2015

Received in revised form 2 October 2015

Accepted 5 October 2015

Available online xxxxx

Keywords:

Fluorogenic probes

Platinum drugs

SAR studies

Platinum(IV) prodrugs

Cisplatin

ABSTRACT

Fluorescence microscopy has emerged as an attractive technique for imaging intracellular Pt species arising from exposure to clinical anticancer drugs such as cisplatin. A rhodamine-B based fluorogenic probe termed **Rho-DDTC** can be activated selectively in the presence of Pt(II) compounds, and possesses the ability to discriminate Pt(II) species from Pt(IV) carboxylate prodrug complexes, thereby providing a unique platform to investigate the reduction of these Pt(IV) complexes after cell entry. In this report, we seek to establish the mechanism of activation of **Rho-DDTC** through a structure–activity relationship study on its structural analogues.

© 2015 Published by Elsevier Inc.

1. Introduction

Pt(II) drugs, namely cisplatin, carboplatin and oxaliplatin are important anticancer compounds used in combination chemotherapy to treat a variety of different malignancies including testicular, ovarian, lung and colorectal cancers (Fig. 1) [1–2]. However, their efficacies are limited by their high toxicity, severe side-effects and occurrences of drug resistance [3–4]. In the context of addressing some of these limitations, Pt(IV) carboxylate complexes have emerged as potential candidates as they are native prodrugs to established Pt(II) agents (Fig. 1). These Pt(IV) prodrug complexes are kinetically inert by virtue of their low-spin d^6 electronic configuration and saturated coordination sphere, but they can be activated to release cytotoxic Pt(II) species upon reduction with concomitant loss of axial carboxylate ligands [5–7]. Consequently, there is a significant body of work directed at exploiting this Pt(IV) scaffold towards developing them as selective Pt anticancer agents with improved therapeutic profiles [8–10].

There is currently a lack of imaging tools capable of directly visualizing the uptake and accumulation of these compounds in cancer cells that would allow investigators to elucidate the mechanisms by which

these Pt-based compounds are processed at the cellular level. Several techniques have been developed to meet this need, centered on determining the elemental Pt composition and the spectroscopic profiles of different Pt oxidation states. An important example would be the use of X-ray adsorption near edge spectroscopy (XANES) to quantitate levels of Pt(IV) and Pt(II) species in tissue samples treated with Pt(IV) prodrugs to investigate intracellular reduction of these prodrugs occurred after cell entry [11]. However, these techniques are generally inaccessible because they require a synchrotron X-ray source and cannot be applied to living cells owing to their destructive nature.

Fluorescence microscopy has emerged as the most effective tool for imaging intracellular Pt species due to its good optical resolution, compatibility with biological systems and availability in most research facilities. However, the technique necessitated the use of a fluorophore as a reporter and consequently, there have been prior attempts to tag fluorescent functional groups to Pt(II)/Pt(IV) scaffolds [12–19]. The main drawback of this system is that the structural modification of the Pt complexes being investigated with bulky organic fluorophores potentially changes the pharmacophore and alters their uptake properties. To circumvent this limitation, our group recently reported a fluorogenic probe based on a rhodamine B (**RhoB**) fluorophore designed to activate selectively in the presence of Pt(II) compounds such as cisplatin [20]. The probe possesses the ability to discriminate Pt(II) species from their parental Pt(IV) prodrugs, thereby providing a platform to investigate the reduction of these Pt(IV) complexes after cell entry. Using confocal microscopy, we showed that Pt(IV) carboxylate prodrug complexes are reduced after cell entry and that there was a difference in intracellular Pt distribution between Pt(IV) and Pt(II) complexes. We

Abbreviations: XANES, X-ray adsorption near edge spectroscopy; ESI-MS, Electrospray ionization mass spectrometry; UV–vis, Ultraviolet–visible; RhoB, rhodamine B; NaDDTC, sodium diethyldithiocarbamate; DDTC, diethyldithiocarbamate; HEPES, 2-[4-(2-hydroxyethyl)piperazin-1-yl]ethanesulfonic acid; DMF, dimethylformamide; DMSO, dimethylsulfoxide; NEt₃, triethylamine; EtOH, ethanol.

* Corresponding author at: Department of Chemistry, National University of Singapore, 3 Science Drive 3, Singapore 117543, Singapore.

E-mail address: chmawh@nus.edu.sg (W.H. Ang).

<http://dx.doi.org/10.1016/j.jinorgbio.2015.10.002>

0162-0134/© 2015 Published by Elsevier Inc.

Please cite this article as: J.X. Ong, et al., Structure–activity relationship studies on rhodamine B-based fluorogenic probes and their activation by anticancer platinum(II) compounds, *J. Inorg. Biochem.* (2015), <http://dx.doi.org/10.1016/j.jinorgbio.2015.10.002>

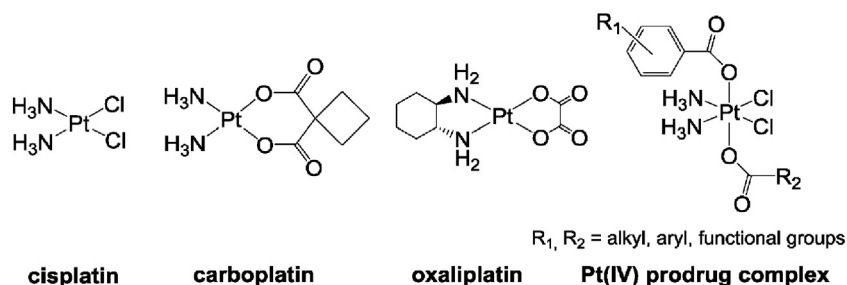


Fig. 1. FDA-approved Pt(II) drugs and representative Pt(IV) carboxylate prodrug complex.

therefore seek to understand the mechanism of probe activation from a structural standpoint, through a structure–activity relationship study centered on a rhodamine B-based fluorogenic probe termed **Rho-DDTC** (Scheme 1), with a view to improve its efficacy towards Pt(II) detection.

2. Experimental section

2.1. Materials and instrumentation

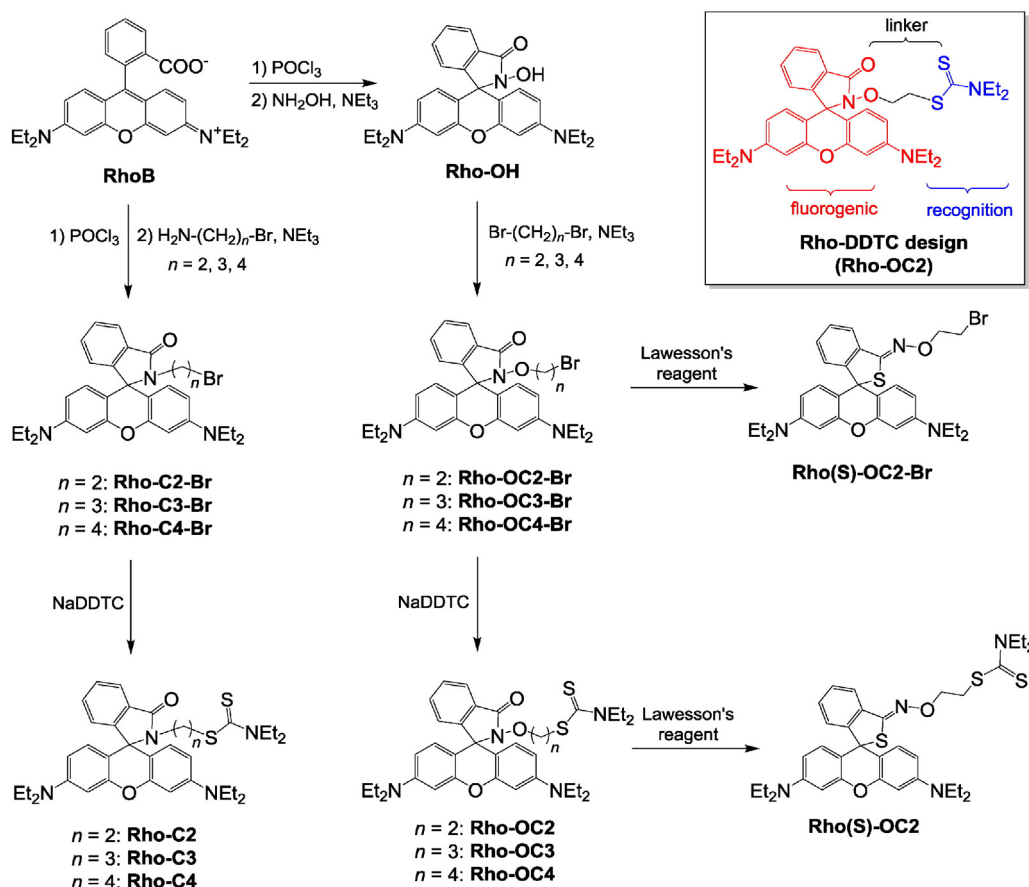
All reagents were purchased from commercial vendors and used without purification. Satraplatin, JM1 18 and oxaliplatin were purchased from Merlin Chemicals Ltd. Cisplatin [21], Pt(en)Cl₂ [22] and oxoplatin [23] were prepared in accordance with literature procedures. **RhoB** hydroxamate (**Rho-OH**) was synthesized according to literature methods [24]. ¹H NMR spectra were recorded on a Bruker Avance 300 MHz model. Chemical shifts are reported in parts per million relative to residual solvent peaks. Electro-spray ionization mass

spectrometry were obtained on a Thermo Finnigan MAT ESI-MS system. UV–vis spectra were recorded on a Shimadzu UV-1800 UV–vis spectrophotometer. Fluorescence spectra were recorded on a Biotek Synergy H1 hybrid multimode plate reader.

2.2. Synthesis of RhoB probes (see Scheme 1 for structures and compound abbreviations)

2.2.1. Synthesis of Rho-OC2

Rho-OH (220 mg, 0.48 mmol) was dissolved in DMF (2 mL) and was added NEt₃ (671 μL, 4.81 mmol) and 1,2-dibromoethane (829 μL, 9.62 mmol). The reaction mixture was heated at 60 °C for 4 h. The solvent was removed and the residue taken up in CH₂Cl₂ (15 mL). The organic mixture was washed with water (10 mL) and NaHCO₃ (10 mL), and dried over Na₂SO₄. The solvent was removed and the crude residue purified by column chromatography (1:3 v/v ethyl acetate:hexane) to yield intermediate compound **Rho-OC2-Br**. Yield: 199 mg (73%, R_f = 0.45). **Rho-OC2-Br** (199 mg, 0.35 mmol) was treated with sodium



Scheme 1. Synthetic route of RhoB fluorescent probes.

diethyldithiocarbamate (NaDDTC) (159 mg, 0.70 mmol) in DMF (2 mL) at r.t. for 12 h. The solvent was removed and the residue was taken up in CH_2Cl_2 (15 mL). The organic mixture was washed with water (10 mL) and brine (10 mL), and dried over Na_2SO_4 . The solvent was removed and the crude residue purified by column chromatography (1:3 v/v ethyl acetate:hexane) to yield the product **Rho-OC2** as white solid. Crystals suitable for single crystal X-ray diffraction analyses were grown via vapor diffusion of diethyl ether into a concentrated CHCl_3 solution. Yield: 204 mg (92%, $R_f = 0.25$). $^1\text{H NMR}$ (300 MHz, CDCl_3): δ 7.92 (1H, d, $J = 5.7$ Hz), 7.47 (2H, m), 7.08 (1H, d, $J = 5.7$ Hz), 6.53–6.56 (2H, m), 6.32–6.38 (4H, m), 3.94–3.98 (4H, m), 3.71 (2H, q, $J = 6.9$ Hz), 3.40 (2H, t, $J = 6.0$ Hz), 3.34 (8H, q, $J = 6.9$ Hz), 1.15–1.29 (18H, m). ESI-MS: m/z 633.2 $[\text{M} + \text{H}]^+$; 655.1 $[\text{M} + \text{Na}]^+$. Anal. calcd. for $\text{C}_{35}\text{H}_{44}\text{N}_4\text{O}_3\text{S}_2$: C 66.42, H 7.01, N 8.85. Found: C 66.15, H 6.64, N 8.87.

2.2.2. Synthesis of **Rho-OC3**

Rho-OH (200 mg, 0.44 mmol), NEt_3 (610 μL , 4.37 mmol) and 1,3-dibromopropane (887 μL , 8.74 mmol) were treated in accordance with the procedure for **Rho-OC2** to yield intermediate **Rho-OC3-Br** as white solid. Yield: 189 mg (75%, $R_f = 0.45$). **Rho-OC3-Br** (189 mg, 0.33 mmol) was reacted with NaDDTC (149 mg, 0.66 mmol) as described in the same procedure to give the product **Rho-OC3** as white solid. Yield: 197 mg (93.1%, $R_f = 0.25$). Crystals suitable for single crystal X-ray diffraction analyses were grown via slow evaporation from a concentrated $\text{CH}_3\text{CN}/\text{CH}_2\text{Cl}_2$ solution. $^1\text{H NMR}$ (300 MHz, CDCl_3): δ 7.92 (1H, d, $J = 5.5$ Hz), 7.49 (2H, m), 7.09 (1H, d, $J = 5.4$ Hz), 6.54–6.57 (2H, m), 6.34–6.43 (4H, m), 3.98 (2H, q, $J = 6.3$ Hz), 3.79 (2H, t, $J = 5.7$ Hz), 3.66 (2H, t, $J = 6.9$ Hz), 3.35 (8H, q, $J = 6.9$ Hz), 3.21 (2H, t, $J = 6.9$ Hz), 1.83 (2H, t, $J = 7.2$ Hz), 1.16–1.59 (18H, m). ESI-MS: m/z 647.2 $[\text{M} + \text{H}]^+$; 669.2 $[\text{M} + \text{Na}]^+$. Anal. calcd. for $\text{C}_{36}\text{H}_{46}\text{N}_4\text{O}_3\text{S}_2$: C 66.84, H 7.17, N 8.66. Found: C 66.77, H 6.83, N 8.46.

2.2.3. Synthesis of **Rho-OC4**

Rho-OH (150 mg, 0.33 mmol), NEt_3 (457 μL , 3.28 mmol) and 1,4-dibromobutane (780 μL , 6.56 mmol) were treated in accordance with the procedure for **Rho-OC2** to yield intermediate **Rho-OC4-Br** as white solid. Yield: 153 mg (78%, $R_f = 0.50$). **Rho-OC4-Br** (153 mg, 0.26 mmol) was reacted with NaDDTC (116 mg, 0.52 mmol) as described in the same procedure to give the product **Rho-OC4** as white solid. Yield: 154 mg (91%, $R_f = 0.30$). $^1\text{H NMR}$ (300 MHz, CDCl_3): δ 7.91 (1H, d, $J = 5.3$ Hz), 7.47 (2H, m), 7.09 (1H, d, $J = 5.7$ Hz), 6.50–6.52 (2H, m), 6.29–6.41 (4H, m), 3.99 (2H, q, $J = 6.6$ Hz), 3.73–3.75 (4H, m), 3.34 (8H, q, $J = 6.3$ Hz), 3.09 (2H, t, $J = 6.6$ Hz), 1.14–1.24 (22H, m). ESI-MS: m/z 661.3 $[\text{M} + \text{H}]^+$; 683.2 $[\text{M} + \text{Na}]^+$. Anal. calcd. for $\text{C}_{37}\text{H}_{48}\text{N}_4\text{O}_3\text{S}_2$: C 67.24, H 7.32, N 8.48. Found: C 67.07, H 6.96, N 8.41.

2.2.4. Synthesis of **Rho(S)-OC2**

Rho-OC2 (100 mg, 0.16 mmol) and Lawesson's reagent (68 mg, 0.17 mmol) were suspended in benzene (8 mL) and refluxed for 2 h. CH_2Cl_2 (10 mL) was added and the reaction mixture was washed with water (2 \times 10 mL). The organic portion was dried over Na_2SO_4 , the solvent removed and the crude residue purified by column chromatography (1:4 v/v ethyl acetate:hexane) to give the product as white solid. Yield: 90.0 mg (85.7%, $R_f = 0.55$). $^1\text{H NMR}$ (300 MHz, CDCl_3): δ 7.88 (1H, d, $J = 6.4$ Hz), 7.33 (2H, m), 7.03 (1H, d, $J = 6.8$ Hz), 6.77–6.79 (2H, m), 6.31 (4H, m), 4.46 (2H, t, $J = 6.4$ Hz), 4.03 (2H, q, $J = 6.8$ Hz), 3.72–3.75 (4H, m), 3.33 (8H, q, $J = 6.8$ Hz), 1.27 (6H, t, $J = 7.2$ Hz), 1.16 (12H, t, $J = 6.8$ Hz). ESI-MS: m/z 649.1 $[\text{M} + \text{H}]^+$. Anal. calcd. for $\text{C}_{35}\text{H}_{44}\text{N}_4\text{O}_2\text{S}_3$: C 64.78, H 6.83, N 8.63. Found: C 64.40, H 6.94, N 8.23.

2.2.5. Synthesis of **Rho(S)-OC2-Br**

Rho-OC2-Br (100 mg, 0.18 mmol) and Lawesson's reagent (72 mg, 0.18 mmol) was reacted in accordance with the earlier procedure to yield **Rho(S)-OC2-Br** as a white solid. Yield: 81.1 mg (78.5%, $R_f = 0.75$). $^1\text{H NMR}$ (300 MHz, CDCl_3): δ 7.85 (1H, d, $J = 6.0$ Hz), 7.35 (2H, m), 7.04 (1H, d, $J = 6.3$ Hz), 6.73–6.78 (2H, m), 6.32 (4H, m),

4.45 (2H, t, $J = 7.2$ Hz), 3.63 (2H, t, $J = 7.2$ Hz), 3.33 (8H, q, $J = 7.2$ Hz), 1.16 (12H, t, $J = 7.2$ Hz). ESI-MS: m/z 580.1 $[\text{M} + \text{H}]^+$. Anal. calcd. for $\text{C}_{30}\text{H}_{34}\text{BrN}_3\text{O}_2\text{S}$: C 62.06, H 5.90, N 7.24. Found: C 61.98, H 6.02, N 7.03.

2.2.6. Synthesis of **Rho-C2**

RhoB·HCl (1 g, 2 mmol) was refluxed in excess POCl_3 (10 mL) for 18 h, after which the solvent was removed to give dark violet-red oil. The crude acid chloride was dissolved in CH_3CN (15 mL), then added 2-bromoethylamine hydrobromide (1 g, 5 mmol) and triethylamine (1.5 mL). The reaction mixture was stirred at r.t. for 24 h, the solvent removed and the organic layer extracted with CH_2Cl_2 (3 \times 20 mL). The organic portions were combined and dried over Na_2SO_4 . The solvent was removed and the crude residue purified by column chromatography (1:3 v/v ethyl acetate:hexane) to give the intermediate compound **Rho-C2-Br** as white solid. Yield: 350 mg (32.0%, $R_f = 0.50$). **Rho-C2-Br** (300 mg, 0.547 mmol) and NaDDTC (246.8 mg, 1.09 mmol) was dissolved in DMF and the reaction mixture was stirred at r.t. for 12 h. The solvent was removed and the residue taken up in CH_2Cl_2 (10 mL). The organic mixture was washed with water (10 mL) and brine (10 mL) and dried over Na_2SO_4 . The solvent was removed and the crude residue purified by column chromatography (1:3 v/v ethyl acetate:hexane) to give the product **Rho-C2** as a white solid. Yield: 311 mg (92.3%, $R_f = 0.30$). Crystals suitable for single crystal X-ray diffraction analyses were grown via slow evaporation from a concentrated $\text{CH}_3\text{CN}/\text{CH}_2\text{Cl}_2$ solution. $^1\text{H NMR}$ (300 MHz, CDCl_3): δ 7.90 (1H, d, $J = 5.7$ Hz), 7.43 (2H, m), 7.07 (1H, d, $J = 6.0$ Hz), 6.29–6.47 (6H, m), 3.91 (2H, q, $J = 6.6$ Hz), 3.62 (2H, q, $J = 6.9$ Hz), 3.47 (2H, t, $J = 6.9$ Hz), 3.32 (8H, q, $J = 7.2$ Hz), 3.11 (2H, t, $J = 5.7$ Hz), 1.14–1.66 (18H, m). ESI-MS: m/z 617.3 $[\text{M} + \text{H}]^+$; 639.3 $[\text{M} + \text{Na}]^+$. Anal. calcd. for $\text{C}_{35}\text{H}_{44}\text{N}_4\text{O}_2\text{S}_2$: C 68.15, H 7.19, N 9.08. Found: C 68.09, H 7.03, N 8.90.

2.2.7. Synthesis of **Rho-C3**

The intermediate **Rho-C3-Br** was prepared in accordance with the procedure for **Rho-C2** using 3-bromopropylamine hydrobromide (1.1 g, 5 mmol) to yield a white solid. Yield: 340 mg (30.3%, $R_f = 0.50$). **Rho-C3-Br** (300 mg, 0.535 mmol) was reacted with NaDDTC (246.3 mg, 1.07 mmol) as described in the same procedure to yield **Rho-C3** as white solid. Yield: 316 mg (93.8%, $R_f = 0.30$). Crystals suitable for single crystal X-ray diffraction analyses were grown via slow evaporation from a concentrated $\text{CH}_3\text{CN}/\text{CH}_2\text{Cl}_2$ solution. $^1\text{H NMR}$ (300 MHz, CDCl_3): δ 7.89 (1H, d, $J = 5.4$ Hz), 7.42 (2H, m), 7.07 (1H, d, $J = 5.7$ Hz), 6.30–6.45 (6H, m), 3.96 (2H, q, $J = 6.6$ Hz), 3.68 (2H, q, $J = 7.2$ Hz), 3.34 (8H, q, $J = 6.9$ Hz), 3.23 (2H, t, $J = 7.2$ Hz), 3.05 (2H, t, $J = 6.9$ Hz), 1.59 (2H, m), 1.17–1.26 (18H, m). ESI-MS: m/z 631.4 $[\text{M} + \text{H}]^+$; 653.4 $[\text{M} + \text{Na}]^+$. Anal. calcd. for $\text{C}_{36}\text{H}_{46}\text{N}_4\text{O}_2\text{S}_2$: C 68.54, H 7.35, N 8.88. Found: C 68.50, H 6.97, N 8.82.

2.2.8. Synthesis of **Rho-C4**

The intermediate **Rho-C4-Br** was prepared in accordance with the procedure for **Rho-C2** using 4-bromobutylamine hydrobromide (1.2 g, 5 mmol) to yield a white solid. Yield: 332 mg (28.9%, $R_f = 0.55$). **Rho-C4-Br** (300 mg, 0.522 mmol) was reacted with NaDDTC (239.4 mg, 1.04 mmol) as described in the same procedure to yield **Rho-C4** as white solid. Yield: 305 mg (90.8%, $R_f = 0.35$). $^1\text{H NMR}$ (300 MHz, CDCl_3): δ 7.90 (1H, d, $J = 5.4$ Hz), 7.43 (2H, m), 7.07 (1H, d, $J = 5.7$ Hz), 6.35–6.48 (6H, m), 3.98 (2H, q, $J = 6.9$ Hz), 3.68 (2H, q, $J = 7.2$ Hz), 3.35 (8H, q, $J = 6.9$ Hz), 3.16 (2H, t, $J = 7.2$ Hz), 3.02 (2H, t, $J = 7.5$ Hz), 1.47 (2H, m), 1.16–1.26 (20H, m). ESI-MS: m/z 645.3 $[\text{M} + \text{H}]^+$; 667.3 $[\text{M} + \text{Na}]^+$. Anal. calcd. for $\text{C}_{37}\text{H}_{48}\text{N}_4\text{O}_2\text{S}_2$: C 68.91, H 7.50, N 8.69. Found: C 68.67, H 7.67, N 8.57.

2.3. Fluorescence determination

All **RhoB** probes were prepared as 1 mM stock solutions in DMSO. Pt(II) complexes were prepared as 1 mM stock solutions in H_2O and

Pt(IV) complexes as 1 mM stock solutions in DMSO. Fluorescence experiments were carried out by incubating RhoB probes (20 μM) with platinum complexes (100 μM) at 37 °C. NaCl, KCl, MgCl_2 , NiCl_2 , CuSO_4 , ZnCl_2 , FeSO_4 , FeCl_3 and K_2PtCl_4 were used as the source of metal ions and prepared as 10 mM stock solutions in water. Selectivity of **Rho(S)-OC2** towards various metal ions was carried out by incubating **Rho(S)-OC2** (20 μM) with metal ions (20 μM) at 25 °C. Selectivity of **Rho(S)-OC2** towards various metal ions at physiological conditions was carried out at 37 °C. Job's plot was carried out with a total [**Rho(S)-OC2**] and $[\text{Pt}^{2+}]$ concentration of 50 μM by varying the mole fraction of Pt^{2+} from 0 to 1. Fluorescence responses of **Rho(S)-OC2** and **Rho-OC2** towards cisplatin were carried out by incubating the probes (20 μM) with cisplatin (100 μM) at 37 °C and fluorescence emission measured at 20 min intervals over a period of 3 h. For all experiments, HEPES buffer (10 mM, pH 7.4, 30% v/v EtOH) was used.

2.4. Determination of solid-state structure

X-ray data for **Rho-C2**, **Rho-OC2** and **Rho-OC3** were collected with a Bruker AXS SMART APEX diffractometer equipped with a CCD camera using Mo K α radiation while **Rho-C3** was measured on a Bruker AXS D8 Venture diffractometer equipped with a Photon 100 CMOS active pixel sensor detector using Cu K α radiation. All data were collected at 100(2) K with the SMART suite of programs. Data were processed and corrected for Lorentz and polarization effects using SAINT software [25], and for absorption effects using the SADABS software [26]. Structural solution and refinement were then carried out using the SHELXTL suite of programs. Structure was solved using Direct methods [27] and subsequent differences Fourier maps, then refined by least squares procedures on weighted F^2 values using the SHELXL-version 2014/6 [28] included in WinGX system programs for Windows [29]. All non-hydrogen atoms were assigned anisotropic displacement parameters. All H atoms were put at calculated positions using the riding model. The detailed crystallographic data is provided in Table S1.

3. Results and discussion

3.1. Synthesis and characterization

The series of compounds were synthesized as shown in Scheme 1 from RhoB as the starting material. RhoB was treated sequentially with POCl_3 and NH_2OH to obtain **Rho-OH**. Linkers with varying chain lengths were installed by the reaction of **Rho-OH** with different dibromoalkanes in the presence of triethylamine as the base. These intermediates were finally treated with NaDDTC to give the desired compounds **Rho-OC2**, **Rho-OC3** and **Rho-OC4**. Treatment of **Rho-OC2** with Lawesson's reagent in benzene afforded **Rho(S)-OC2**. As the C=S double bond is weak, **Rho(S)-OC2** is expected to exist predominately as tautomer B (Fig. S9) [30–31]. Prevalence of the thioether tautomer in solution was consistent with the detection of a single species in ^1H NMR and the downfield shift of the methylene resonances on the linker motif, indicating a change in chemical environment. Furthermore, the IR spectrum of **Rho(S)-OC2** also exhibited a distinct C=N stretch at 1613.5 cm^{-1} (Fig. S20). Reaction of RhoB with POCl_3 followed by 2-bromoethylamine, 3-bromopropylamine and 4-bromobutylamine, respectively in the presence of triethylamine, yielded bromo-terminated Rho-B amides which were subsequently treated with NaDDTC to yield **Rho-C2**, **Rho-C3** and **Rho-C4**. All the final compounds were analyzed and fully characterized by ^1H NMR, ESI-MS as well as X-ray crystallographic analyses.

Single crystals of **Rho-C2**, **Rho-C3** and **Rho-OC3** suitable for X-ray diffraction studies were obtained from slow evaporation of concentrated $\text{CH}_3\text{CN}/\text{CH}_2\text{Cl}_2$ solutions of the compounds whereas single crystals of **Rho-OC2** were grown by vapor diffusion of diethyl ether into a concentrated CHCl_3 solution. The solid-state structures of **Rho-C2**, **Rho-C3**, **Rho-OC2** and **Rho-OC3** revealed that these compounds exist as

closed-ring spirolactams (Fig. 2). The core RhoB and DDTC structures remained intact, with key bond distances and angles largely the same. The key difference is the separation of the DDTC recognition motif from the spirolactam ring due to variations in linker length. The straight-line separation between DDTC and spirolactam through-space, measured from N3 to S1, were determined to be 4.071 Å, 5.230 Å, 5.006 Å and 5.731 Å for **Rho-C2**, **Rho-C3**, **Rho-OC2** and **Rho-OC3**, respectively, while the cumulative through-bond distances from N3 to S1 were 4.782 Å, 6.295 Å, 6.151 Å and 7.673 Å (Table 1). The solid-state structures for **Rho-C3** and **Rho-OC2** are remarkably similar with differences in the N3–S1 separation arising from shorter N–O/C–O bond lengths in **Rho-OC2** due to the hydroxamate linkage, compared to N–C/C–C bond lengths in **Rho-C3**.

3.2. Structure–activity relationship studies

We hypothesized that recognition of cisplatin by **Rho-DDTC** probe proceeded via a 2-step activation process culminating in spiro-ring opening. First, the DDTC recognition motif reacted with cisplatin resulting in mono-substitution by the thiocarbonyl group. The thiocarbonyl group on the DDTC recognition motif labilises the *trans*-ligand via *trans*-effect which resulted in subsequent reactivity with the spirolactam on RhoB. This reaction relieved the ring strain via spiro-ring opening and enabled fluorescence turn-on. To establish the validity of this hypothesis, we prepared structurally analogous **Rho-DDTC** probes with varying linker chain lengths namely **Rho-OC2**, **Rho-OC3** and **Rho-OC4**. We reasoned that increasing linker length would prevent cooperativity between the DDTC recognition motif and the fluorophore, eventually leading to reduced probe activation.

RhoB probes were treated with cisplatin (5 \times eq.) in HEPES buffer (10 mM, pH 7.4, 30% v/v EtOH). A marked decrease in both fluorescence and absorbance were observed for **Rho-OC3** and **Rho-OC4** comprising 4-atom and 5-atom linker lengths between DDTC and spirolactam, respectively, compared to prototypical **Rho-OC2** which has 3-atom linkage (Figs. 3, S1). Similar trends were observed when JM118 (5 \times eq.) was utilized. JM118 is the Pt(II) congener of Pt(IV) prodrug candidate satraplatin, currently undergoing Phase III clinical trials for hormone-refractory prostate cancer. The results indicated that the probes were poorly activated in the presence of cisplatin due to the increased length of the linker, validating our hypothesis. Thus after initial binding of cisplatin to the probe through DDTC, subsequent nucleophilic attack on Pt by the spirolactam motif was less likely since the extended linker chain would put it out of reach from the spirolactam. In addition, the difference in probe activation also suggested that spiro-ring opening was preceded by DDTC recognition of cisplatin, not vice-versa. Otherwise, the three probes would have displayed similar levels of reactivity by virtue of their common RhoB core structures.

We replaced the hydroxamate group on the probe with the amide with a view to tune their reactivity towards Pt complexes and to further simplify the synthesis. A marked reduction in fluorescence turn-on was observed for **Rho-C3** compared to **Rho-OC2**, even though both comprised 3-atom linkers, suggesting that the hydroxamate O-atom played a crucial role in the ring opening reaction. This was presumably due to the electron-donating O atom stabilizing the formation of the carboximidate group following complexation and ring-opening. In its absence, spirolactam **Rho-C3** preferentially adopted the amide functionality and was therefore less susceptible towards ring-opening (Fig. S10). Intriguingly, low levels of probe activation were observed when the linker length was reduced i.e. **Rho-C2** with 2-atom linker. This was because the short linker length would exert a considerable strain on ring formation with cisplatin bound to both DDTC and RhoB leading to an unfavorable binding conformation. In keeping with **Rho-OC3**, **Rho-C4** exhibited lower probe activation compared to **Rho-C3** due to increased separation between the recognition motif and the spirolactam fluorophore. All in all, the results pointed to the linker

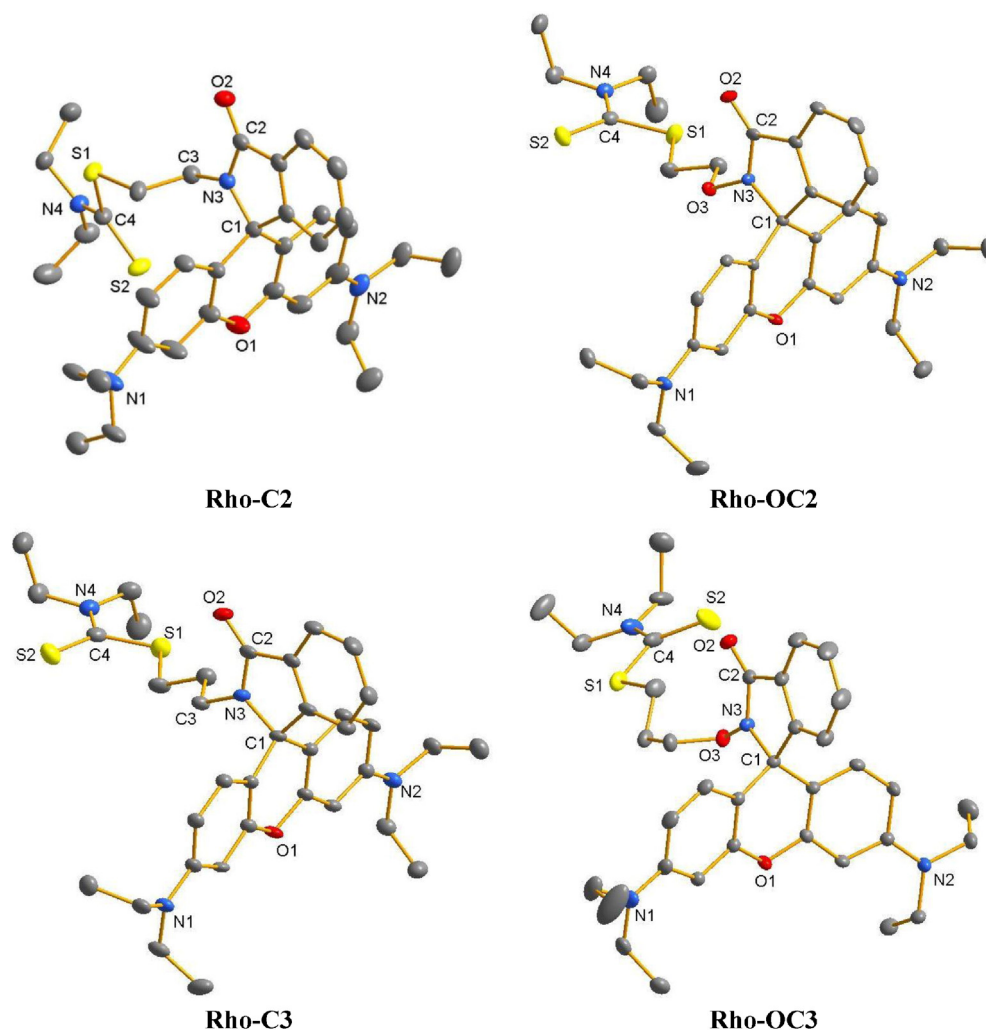


Fig. 2. Molecular representation of selected RhoB probes; atoms are represented as thermal ellipsoids at 50% probability. Hydrogen atoms are omitted for clarity.

length being an important parameter for the efficacy of this class of fluorogenic probes with a 3-atom linkage being the optimal separation.

3.3. Thionylation of spirolactam to enhance reactivity

In order to increase levels of probe activation, we investigated whether introducing sulfur-based functional groups at the spirolactam

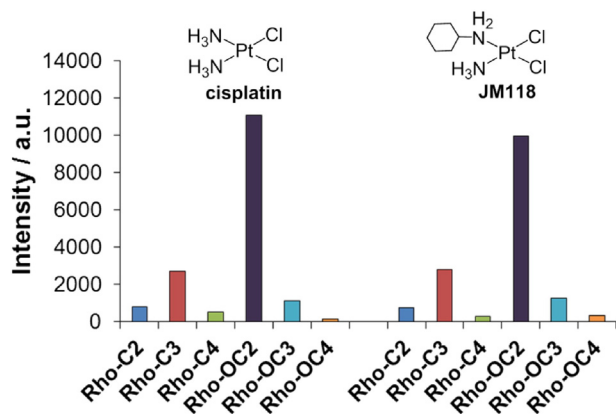


Fig. 3. Fluorescence responses ($\lambda_{\text{ex}} = 500 \text{ nm}$, $\lambda_{\text{em}} = 595 \text{ nm}$) of RhoB compounds (20 μM) after treatment with cisplatin and JM118 in HEPES buffer (10 mM, pH 7.4, 30% v/v EtOH).

component would enhance the overall reactivity of the probe. We reasoned that a soft S-atom at the fluorophore would bind more strongly with the soft Pt metal centre in the second nucleophilic attack by the spirolactam, thereby promoting spiro-ring opening and consequently, increasing fluorescence turn-on. Therefore, **Rho-OC2** was converted quantitatively to **Rho(S)-OC2** using the Lawesson's reagent with concomitant conversion to its thioether tautomer. Encouragingly, **Rho(S)-OC2** exhibited ca. 4-fold increase in fluorescence compared to **Rho-OC2** when treated with cisplatin under the same reaction conditions (Figs. 4, S2), with a slight shift in λ_{max} . This is accompanied by higher UV–vis absorbance levels with a more intense color change which could be observed visually (Fig. 5). A more rapid probe response was also noted with fluorescence turn-on registered within 20 min of reaction time for **Rho(S)-OC2** compared to **Rho-OC2** which required at least 120 min (Fig. S4). This significantly-enhanced sensitivity and reactivity towards cisplatin could make it an ideal fluorogenic probe for real-time imaging of Pt drugs within living cells. A similar trend in the fluorescence and absorbance properties was also observed when the probes were treated with JM118.

3.4. Selectivity of thionylated probe **Rho(S)-OC2**

We proceeded to establish whether the DDTC recognition motif was essential for probe activation in this tautomeric thioether form of **Rho(S)-OC2**, since there was a distinct possibility that probe activation would proceed via reaction of thioether with cisplatin, potentially

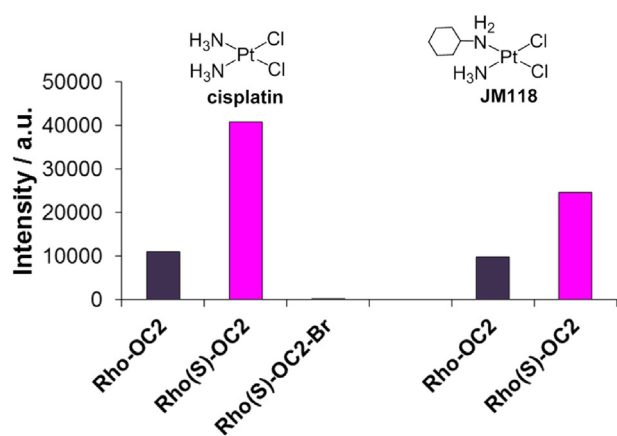


Fig. 4. Fluorescence responses ($\lambda_{\text{ex}} = 500 \text{ nm}$, $\lambda_{\text{em}} = 595 \text{ nm}$) of **Rho-OC2**, **Rho(S)-OC2** and **Rho(S)-OC2-Br** ($20 \mu\text{M}$) after treatment with cisplatin and JM118 in HEPES buffer (10 mM , $\text{pH } 7.4$, $30\% \text{ v/v EtOH}$).

rendering the probe unselective. Therefore, intermediate **Rho-OC2-Br**, which contained the 3-atom linker but without the DDTc recognition motif, was treated with Lawesson's reagent to yield **Rho(S)-OC2-Br** as a negative control. When exposed to cisplatin under the same conditions, **Rho(S)-OC2-Br** only yielded basal fluorescence values indicating that there was no reactivity (Fig. 4), thereby pointing out that initial DDTc binding was essential for the probe activation of **Rho(S)-OC2**. We concluded that the mechanism of action involved in the activation of **Rho(S)-OC2** by cisplatin was akin to that for **Rho-OC2**, with a recognition step for selective Pt-binding followed by spiro-ring opening (Fig. S11). Indeed despite its enhanced reactivity, the selectivity of **Rho(S)-OC2** towards Pt^{2+} was high compared to other metal ions such as Na^+ , K^+ , Cu^{2+} , Ni^{2+} , Zn^{2+} , Fe^{2+} and Fe^{3+} which play important roles in biological systems (Fig. S6). Analysis of a Job's plot indicated maximum fluorescence intensity at a mole fraction of 0.5, which suggests that **Rho(S)-OC2** interacted with Pt^{2+} in a 1:1 ratio (Fig. S5). Selectivity for cisplatin was high at elevated concentrations of other physiologically-relevant metal ions i.e. Na^+ , K^+ and Mg^{2+} (15 mM) making it a suitable intracellular probe (Fig. S7). Linear fluorescence turn-on response to the probe was observed at clinically-relevant cisplatin concentrations between $20\text{--}100 \mu\text{M}$ (Fig. S8).

With this more reactive **Rho(S)-OC2** probe in hand, we investigated whether it could be activated in the presence of Pt(II) complexes containing chelating amine ligands which was previously shown not to activate **Rho-OC2** due to the stable amine chelate. Treatment of **Rho(S)-OC2** with $\text{Pt}(\text{en})\text{Cl}_2$ and oxaliplatin showed no activation of the probe as indicated by baseline fluorescence signals (Fig. 6). Since the recognition motif remains unchanged in this novel compound and the initial step has been determined to be binding of DDTc to Pt metal

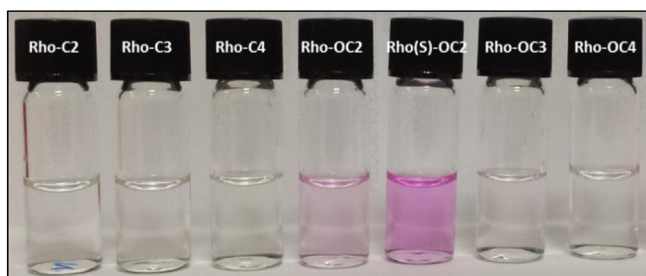


Fig. 5. Color changes of RhoB probes ($20 \mu\text{M}$) after treatment with cisplatin in HEPES buffer (10 mM , $\text{pH } 7.4$, $30\% \text{ v/v EtOH}$). Only **Rho-OC2** and **Rho(S)-OC2** displayed visible color changes after incubation with cisplatin.

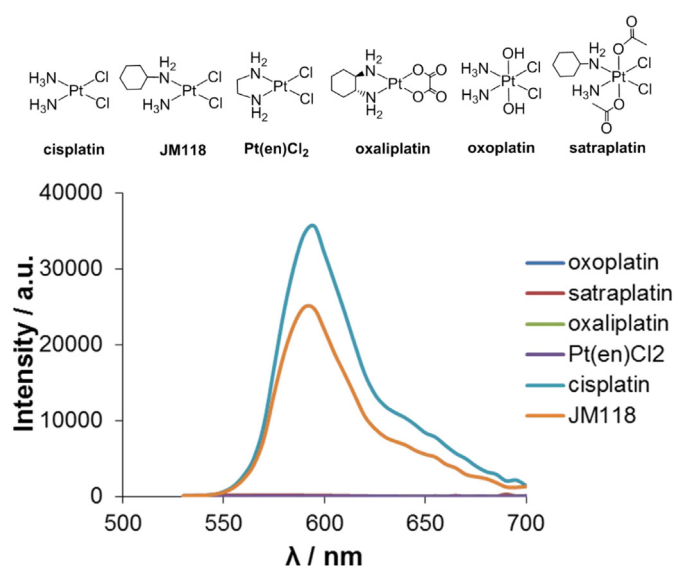


Fig. 6. Fluorescence spectra ($\lambda_{\text{ex}} = 500 \text{ nm}$, $\lambda_{\text{em}} = 595 \text{ nm}$) of **Rho(S)-OC2** ($20 \mu\text{M}$) after treatment with Pt(II) and Pt(IV) complexes in HEPES buffer (10 mM , $\text{pH } 7.4$, $30\% \text{ v/v EtOH}$).

center, having a more reactive thiospiroactam would not result in activation of the probe. In the absence of DDTc binding to Pt metal center, the probe was not activated. Lastly, we also investigated the ability of **Rho(S)-OC2** to distinguish between Pt(II) drugs and their parental Pt(IV) complexes (Fig. 6). Both oxoplatin and satraplatin which are based on cisplatin and JM118 templates respectively did not trigger any fluorescence turn on. This clearly shows that the probe is able to differentiate between Pt(II) and Pt(IV) metal centers which makes it an ideal tool to study the reduction of Pt(IV) prodrugs in biological systems. Pt(IV) prodrugs are known to undergo intracellular reduction to generate Pt(II) species to release its cytotoxic effects on cancer cells. With the rapid activation of **Rho(S)-OC2** by Pt(II) species, it would be feasible to adopt this probe to study real-time reduction of Pt(IV) prodrugs to Pt(II) species within living cells.

4. Conclusion

A series of RhoB fluorescent probes were synthesized to study the mechanism of action for the activation of these probes in the presence of Pt(II) drugs such as cisplatin and JM118. The probe **Rho-OC2** undergoes a two-step activation process involving binding of the substrate to the recognition motif, followed by reactivity with the RhoB spiroactam as proposed previously. Extending or contracting the distances between the DDTc recognition motif and the fluorophore led to a decrease in probe activation, indicating that they are both cooperatively involved. Thionylation of the spiroactam functional group led to formation of the thioether tautomer which significantly enhanced the reactivity of **Rho(S)-OC2** towards Pt(II) complexes; presumably by promoting nucleophilic attack on the Pt metal center in the second step. The high selectivity of the probe was preserved as **Rho(S)-OC2** could effectively distinguish between Pt(IV) prodrug complexes and their Pt(II) products, making it an ideal tool to study the reduction of Pt(IV) prodrugs within living cells.

Acknowledgments

Financial support from the Ministry of Education (R143-000-572-112) and the National University of Singapore is gratefully acknowledged.

Appendix A. Supplementary data

Supplementary data to this article can be found online at <http://dx.doi.org/10.1016/j.jinorgbio.2015.10.002>.

References

- [1] B. Rosenberg, L. Van Camp, T. Krigas, *Nature* 205 (1965) 698–699.
- [2] B. Rosenberg, L. Vancamp, J.E. Trosko, V.H. Mansour, *Nature* 222 (1969) 385–386.
- [3] M.A. Fuertes, C. Alonso, J.M. Pérez, *Chem. Rev.* 103 (2003) 645–662.
- [4] M.A. Fuertes, J. Castilla, C. Alonso, J.M. Perez, *Curr. Med. Chem.* 2 (2002) 539–551.
- [5] M.D. Hall, H.R. Mellor, R. Callaghan, T.W. Hambley, *J. Med. Chem.* 50 (2007) 3403–3411.
- [6] J.S. Butler, P.J. Sadler, *Curr. Opin. Chem. Biol.* 17 (2013) 175–188.
- [7] O. Nováková, O. Vrána, V.I. Kiseleva, V. Brabec, *Eur. J. Biochem.* 228 (1995) 616–624.
- [8] W.H. Ang, I. Khalaila, C.S. Allardyce, L. Juillerat-Jeanneret, P.J. Dyson, *J. Am. Chem. Soc.* 127 (2005) 1382–1383.
- [9] K.R. Barnes, A. Kutikov, S.J. Lippard, *Chem. Biol.* 11 (2004) 557–564.
- [10] L. Ma, R. Ma, Y. Wang, X. Zhu, J. Zhang, H.C. Chan, X. Chen, W. Zhang, S.K. Chiu, G. Zhu, *Chem. Commun.* 51 (2015) 6301–6304.
- [11] M.D. Hall, G.J. Foran, M. Zhang, P.J. Beale, T.W. Hambley, *J. Am. Chem. Soc.* 125 (2003) 7524–7525.
- [12] R.A. Alderden, H.R. Mellor, S. Modok, T.W. Hambley, R. Callaghan, *Biochem. Pharmacol.* 71 (2006) 1136–1145.
- [13] N.S. Bryce, J.Z. Zhang, R.M. Whan, N. Yamamoto, T.W. Hambley, *Chem. Commun.* (2009) 2673–2675.
- [14] S. Ding, X. Qiao, J. Suryadi, G.S. Marrs, G.L. Kucera, U. Bierbach, *Angew. Chem. Int. Ed.* 52 (2013) 3350–3354.
- [15] Y. Song, K. Suntharalingam, J.S. Yeung, M. Royzen, S.J. Lippard, *Bioconjug. Chem.* 24 (2013) 1733–1740.
- [16] J.J. Wilson, S.J. Lippard, *Inorg. Chim. Acta* 389 (2012) 77–84.
- [17] Y. Yuan, Y. Chen, B.Z. Tang, B. Liu, *Chem. Commun.* 50 (2014) 3868–3870.
- [18] E.J. New, R. Duan, J.Z. Zhang, T.W. Hambley, *Dalton Trans.* (2009) 3092–3101.
- [19] C. Molenaar, J.-M. Teuben, R.J. Heetebrij, H.J. Tanke, J. Reedijk, *J. Biol. Inorg. Chem.* 5 (2000) 655–665.
- [20] D. Montagner, S.Q. Yap, W.H. Ang, *Angew. Chem. Int. Ed.* 52 (2013) 11785–11789.
- [21] S.C. Dhara, *Ind. J. Chem.* 8 (1970) 193–194.
- [22] C.K. Chen, J.Z. Zhang, J.B. Aitken, T.W. Hambley, *J. Med. Chem.* 56 (2013) 8757–8764.
- [23] W.H. Ang, S. Pilet, R. Scopelliti, F. Bussy, L. Juillerat-Jeanneret, P.J. Dyson, *J. Med. Chem.* 48 (2005) 8060–8069.
- [24] X. Chen, J. Jia, H. Ma, S. Wang, X. Wang, *Anal. Chim. Acta* 632 (2009) 9–14.
- [25] Saint program included in the package software: APEX v2014.11.0.
- [26] N. Walker, D. Stuart, *Acta Crystallogr. A* 39 (1983) 158–166.
- [27] G.M. Sheldrick, *Acta Crystallogr. A* 71 (2015) 3–8.
- [28] G.M. Sheldrick, *Acta Crystallogr. A* 64 (2008) 112–122.
- [29] L.J. Farrugia, *J. Appl. Crystallogr.* 32 (1999) 837–838.
- [30] M.Y. Chae, A.W. Czarnik, *J. Am. Chem. Soc.* 114 (1992) 9704–9705.
- [31] W. Huang, C. Song, C. He, G. Lv, X. Hu, X. Zhu, C. Duan, *Inorg. Chem.* 48 (2009) 5061–5072.